JAERI-M
88-123

PRESENT STATUS OF JT-60 ICRF HEATING EXPERIMENT

July 1988

Haruyuki KIMURA, Tsuneyuki FUJII, Mikio SAIGUSA
Kiyotaka HAMAMATSU, Yoshinori KUSAMA, Kenji TOBITA
Masahiro NEMOTO, Keisuke NAGASHIMA, Noriyuki KOBAYASHI
Shinichi MORIYAMA, Yoshio OGAWA, Katsuto ANNO
Shinichi SHINOZAKI, Masayuki TERAKADO and JT-60 Team

日本原子力研究所
Japan Atomic Energy Research Institute

JAERI-Mレポートは，日本原子力研究所が不定期に公刊している研究報告書です。
入手の問合わせは，日本原子力研究所技術情報部情報資料課（〒319-11茨城県那珂郡東海村）あて，お申しこしください。なお，このほかに財団法人原子力弘済会資料センター（〒319-11 茨城県那珂郡東海村日本原子力研究所内）で複写による実費頒布をおこなっております。

JAERI-M reports are issued irregularly.
Inquiries about availability of the reports should be addressed to Information Division Department of Technical Information, Japan Atomic Energy Research Institute, Tokai-mura, Naka-gun, Ibaraki-ken 319-11, Japan.

編集兼発行　日本原子力研究所
印　　刷　㈱高野高速印刷

Present Status of JT-60 ICRF Heating Experiment

Haruyuki KIMURA[+1], Tsuneyuki FUJII[+2], Mikio SAIGUSA[+2]
Kiyotaka HAMAMATSU, Yoshinori KUSAMA, Kenji TOBITA
Masahiro NEMOTO, Keisuke NAGASHIMA, Noriyuki KOBAYASHI[+2]
Shinichi MORIYAMA[+3], Yoshio OGAWA[+3], Katsuto ANNO[+3]
Shinichi SHINOZAKI[+3], Masayuki TERAKADO[+3] and JT-60 Team

Department of Large Tokamak Research
Naka Fusion Research Establishment
Japan Atomic Energy Research Institute
Naka-machi, Naka-gun, Ibaraki-ken

(Received June 9, 1988)

Recent results on JT-60 ion-cyclotron-range-of-frequency (ICRF) heating experiment in the second harmonic regime are reviewed. Remarkable beam acceleration by second harmonic ICRF wave was observed during combined heating with neutral-beam-injection (NBI). Incremental energy confinement time of ICRF up to 210 msec was obtained with beam acceleration, which is about three times as high as that of NBI or ICRF heating alone case. Second harmonic ICRF heating is also effective in ohmic target plasma with antenna phasing in the toroidal direction. Antenna coupling properties during H-mode were investigated. Coupling resistance increased after H-transition in $(\pi,0)$ mode. Future plan for upgrade of the JT-60 ICRF heating system is also presented.

Keywords; JT-60, Second Harmonic ICRF Heating, Beam Acceleration, NBI, Incremental Energy Confinement Time, Antenna Phasing, Coupling Resistance, H-mode

---

+1 Fusion Experimental Reactor Team
+2 Department of Thermonuclear Fusion Research
+3 Department of JT-60 Facility

ＪＴ－６０　ＩＣＲＦ加熱実験の現状

日本原子力研究所那珂研究所臨界プラズマ研究部
木村　晴行[+1]・藤井　常幸[+2]・三枝　幹雄[+2]
濱松　清隆・草間　義紀・飛田　健次
根本　正博・永島　圭介・小林　則幸[+2]
森山　伸一[+3]・小川　芳郎[+3]・安納　勝人[+3]
篠崎　信一[+3]・寺門　正之[+3]・ＪＴ－６０チーム

（１９８８年６月９日受理）

ＪＴ－６０第２調波イオンサイクロトロン周波数帯（ＩＣＲＦ）加熱実験の最近の成果についてまとめた。中性粒子入射（ＮＢＩ）加熱との組合せ加熱時に第２調波ＩＣＲＦ波による顕著なビーム加速が観測された。ビーム加速に伴いＩＣＲＦの〝エネルギー増分閉じ込め時間〟は２１０msec に達した。この値はＮＢＩ又はＩＣＲＦの単独加熱時の値の約３倍に相当する。第２調波ＩＣＲＦ加熱はオーム加熱プラズマに対してもトロイダル方向のアンテナ位相制御により有効である。Ｈモード時のアンテナ結合特性について調べられた。（π，０）モードに於いては結合抵抗はＨモード遷移後，増加する。ＪＴ－６０　ＩＣＲＦ加熱装置の増力計画について最後に触れる。

那珂研究所：〒311-01 茨城県那珂郡那珂町大字向山 801-1
＋１　核融合実験炉特別チーム
＋２　核融合研究部
＋３　ＪＴ－６０試験部

Contents

1. Introduction 1
2. JT-60 ICRF Heating System 2
3. Antenna Coupling Resistance 2
4. Radiation Loss during ICRF Heating 3
5. Beam Acceleration during Combined NBI and ICRF Heating 3
5.1 Introduction 3
5.2 Parameter Survey 4
5.3 Beam Acceleration under Optimized Conditions 5
5.4 Enhancement of τ_E^{inc} with Beam Acceleration 6
6. ICRF Heating of OH Plasma 7
7. Antenna-Plasma Coupling during H-mode 7
8. Summary 8
9. Experimental Programme in 1988 8
10. Future Plan 8
Acknowledgement 9
References 9

目　　次

1. 序論…… 1
2. ＪＴ－６０　ＩＣＲＦ加熱装置…… 2
3. アンテナ結合抵抗…… 2
4. ＩＣＲＦ加熱時の放射損失…… 3
5. ＮＢＩとＩＣＲＦ組合せ加熱時のビーム加速…… 3
5.1 序論…… 3
5.2 パラメータサーベイ…… 4
5.3 最適条件下のビーム加速…… 5
5.4 ビーム加速に伴うτ_E^{inc}の増大…… 6
6. オーム加熱プラズマのＩＣＲＦ加熱…… 7
7. Ｈモード時のアンテナープラズマ結合…… 7
8. まとめ…… 8
9. １９８８年度の実験計画…… 8
10. 将来計画…… 8
謝辞…… 9
参考文献…… 9

1. Introduction

Second harmonic ion-cyclotron-range-of-frequency (ICRF) heating is now being investigated in the JT-60 tokamak[1]. The second harmonic ICRF heating is attractive, because it can heat majority ions predominantly and its power deposition profile can be much narrower than that of neutral-beam-injection (NBI) heating. Fusion product $\langle n_e \tau_E T_i \rangle$ can be expected to rise thus more efficiently by second harmonic ICRF heating than by NBI heating, assuming same transport coefficient in both cases.

Construction of JT-60 ICRF heating system[2] has been completed substantially in July, 1986. Antenna conditioning in vacuum has begun since August, 1986. The voltage stand-off in the launching system has reached 45 kV with pulse duration of 3 seconds up to now. The heating experiment has started from September, 1986. Since then, we have had three experimental periods. The first priority on JT-60 experiment for these periods, however, was put on high power NBI heating experiment. Therefore, number of experimental shots given for ICRF was restricted within only about 100 shots in each period. Nonetheless, some important results has been obtained in JT-60 ICRF experiment. Main experimental results in each period are summarized as follows.

(1) September - November, 1986

Coupling properties of the 2×2 phased loop array was investigated for various phasing modes[3]. Coupling resistance, R_c up to 10 Ω was obtained for (0,0) mode*). Cavity resonance was observed in (0,0) mode. Moreover, it was found that the cavity resonance was supressed with (π,0) mode, which is consistent with theoretical analysis[4].

Preliminary result on the beam acceleration was obtained during combined NBI and ICRF heating.

(2) January - March, 1987

Optimization of the heating and the beam acceleration with $k_{\parallel}$-shaping (phase control in the toroidal direction) was investigated[5]. The incremental energy confinement time for (π,0) mode was 70 msec, while the one for (0,0) mode was only 40 msec. Efficiency of the beam acceleration for (π,0) mode was also twice as high as the one of (0,0) mode. Parameter survey on the beam acceleration was made and the optimum condition for the beam acceleration was clarified[5].

---

*) ($\Delta\varphi$,$\Delta\theta$) denotes the phase difference of the 2×2 loop array. $\Delta\varphi$ is the toroidal phase difference and $\Delta\theta$ the poloidal one.

The maximum torus input power reached 2.1 MW, which corresponds to the power density of the antenna of 1.1 kW/cm^2. This value is close to the best value of the power density of the ICRF antennas of tokamaks in the world[6].

(3) July - October, 1987[7]

The material of the first wall and the antenna guard limiter has been changed from molybdenum coated by TiC to carbon in May, 1987. As a result, the radiation loss during ICRF heating has been reduced significantly.

Enhanced confinement associated with beam acceleration was observed during combined NBI and ICRF heating. Antenna coupling properties during H-mode was investigated. It was found that the coupling resistance increased after H-mode transition for (π,0) phasing. This result implies that the coupling resistance can be controlled with antenna phase control even for the H-mode plasma.

This paper describes the present status of the JT-60 ICRF experiment, centering around the experimental results in the second and third experimental periods. Future plan for the JT-60 ICRF heating system is also mentioned.

2. JT-60 ICRF Heating System

Outline of the JT-60 ICRF heating system is only briefly described here. Detailed description is given in Refs. 2 and 8. Frequency range is 108 - 132 MHz, which corresponds to the second harmonic cyclotron resonance frequency of hydrogen for a range of the toroidal magnetic field of JT-60. Experiment has been done at 120 MHz up to the last experimental period. Generator output power is 6 MW, which is delivered by eight lines of amplifier chain. A coupler is 2×2 phased loop antenna. Schematic view of the antenna is shown in Fig. 1. One of the feature of this coupler is open-type Faraday shield[9]. Up to now, we have observed no adverse effects on the open-type Faraday shield. Material of the guard limiter has been changed from molybdenum coated by TiC to carbon in May, 1987.

3. Antenna Coupling Resistance

We have used mainly two phasing modes so far. One is (0,0) mode. Phase difference is zero both in toroidal and poloidal directions. The

The maximum torus input power reached 2.1 MW, which corresponds to the power density of the antenna of 1.1 kW/cm^2. This value is close to the best value of the power density of the ICRF antennas of tokamaks in the world[6].

(3) July - October, 1987[7]

The material of the first wall and the antenna guard limiter has been changed from molybdenum coated by TiC to carbon in May, 1987. As a result, the radiation loss during ICRF heating has been reduced significantly.

Enhanced confinement associated with beam acceleration was observed during combined NBI and ICRF heating. Antenna coupling properties during H-mode was investigated. It was found that the coupling resistance increased after H-mode transition for (π,0) phasing. This result implies that the coupling resistance can be controlled with antenna phase control even for the H-mode plasma.

This paper describes the present status of the JT-60 ICRF experiment, centering around the experimental results in the second and third experimental periods. Future plan for the JT-60 ICRF heating system is also mentioned.

2. JT-60 ICRF Heating System

Outline of the JT-60 ICRF heating system is only briefly described here. Detailed description is given in Refs. 2 and 8. Frequency range is 108 - 132 MHz, which corresponds to the second harmonic cyclotron resonance frequency of hydrogen for a range of the toroidal magnetic field of JT-60. Experiment has been done at 120 MHz up to the last experimental period. Generator output power is 6 MW, which is delivered by eight lines of amplifier chain. A coupler is 2×2 phased loop antenna. Schematic view of the antenna is shown in Fig. 1. One of the feature of this coupler is open-type Faraday shield[9]. Up to now, we have observed no adverse effects on the open-type Faraday shield. Material of the guard limiter has been changed from molybdenum coated by TiC to carbon in May, 1987.

3. Antenna Coupling Resistance

We have used mainly two phasing modes so far. One is (0,0) mode. Phase difference is zero both in toroidal and poloidal directions. The

The maximum torus input power reached 2.1 MW, which corresponds to the power density of the antenna of 1.1 kW/cm^2. This value is close to the best value of the power density of the ICRF antennas of tokamaks in the world[6].

(3) July - October, 1987[7]

The material of the first wall and the antenna guard limiter has been changed from molybdenum coated by TiC to carbon in May, 1987. As a result, the radiation loss during ICRF heating has been reduced significantly.

Enhanced confinement associated with beam acceleration was observed during combined NBI and ICRF heating. Antenna coupling properties during H-mode was investigated. It was found that the coupling resistance increased after H-mode transition for (π,0) phasing. This result implies that the coupling resistance can be controlled with antenna phase control even for the H-mode plasma.

This paper describes the present status of the JT-60 ICRF experiment, centering around the experimental results in the second and third experimental periods. Future plan for the JT-60 ICRF heating system is also mentioned.

2. JT-60 ICRF Heating System

Outline of the JT-60 ICRF heating system is only briefly described here. Detailed description is given in Refs. 2 and 8. Frequency range is 108 - 132 MHz, which corresponds to the second harmonic cyclotron resonance frequency of hydrogen for a range of the toroidal magnetic field of JT-60. Experiment has been done at 120 MHz up to the last experimental period. Generator output power is 6 MW, which is delivered by eight lines of amplifier chain. A coupler is 2×2 phased loop antenna. Schematic view of the antenna is shown in Fig. 1. One of the feature of this coupler is open-type Faraday shield[9]. Up to now, we have observed no adverse effects on the open-type Faraday shield. Material of the guard limiter has been changed from molybdenum coated by TiC to carbon in May, 1987.

3. Antenna Coupling Resistance

We have used mainly two phasing modes so far. One is (0,0) mode. Phase difference is zero both in toroidal and poloidal directions. The

other is (π,0) mode. Phase difference is 180 degrees in toroidal direction and zero in poloidal direction. Typical example of calculation of antenna radiation power spectra for two phasing modes is shown in Fig. 2. The peak position of the spectra is 0 m^{-1} for (0,0) mode and about 10 m^{-1} for (π,0) mode.

Figure 3 shows dependence of the antenna coupling resistance on the line-averaged electron density. The coupling resistance of (0,0) mode is in the range of 4 - 10 Ω and the one of (π,0) mode is 1 - 4 Ω. Previously, we observed large asymmetry of the coupling resistance between upper and lower loops. Recently, we have found that the coupling resistances can be equalized by adjusting the stub tuners. The difference is due to the mutual coupling between the upper and lower loops. The antenna-side stub of the double stub tuners plays an important role in adjusting the mutual coupling. The equalized values are also shown in Fig. 3 by $\ominus$ and $\bullet$ for (0,0) mode and $\circ$ for (π,0) mode. These are located between the previous data of upper and lower loops. Results of the coupling calculation are also shown. Experimental values are in general agreement with the calculated ones.

4. Radiation Loss during ICRF Heating

The radiation loss during ICRF heating has been reduced significantly by replacement of the first wall and the antenna guard limiter with carbon ones. Table 1 compares $\Delta P_{rad}/P_{IC}$, a ratio of the incremental radiation loss associated with ICRF heating to the ICRF power, before and after the replacement.

In the case of TiC wall, $\Delta P_{rad}/P_{IC}$ is dependent on the electron density, phase control and target plasma condition. $\Delta P_{rad}/P_{IC}$ reached about 2 in the low density and ohmic target plasma. This is the worst case. It was reduced with increasing density or injecting neutral beam. After replacement with carbon wall, it has been reduced significantly even in the low density and ohmic target plasma.

5. Beam acceleration during Combined NBI and ICRF Heating

5.1 Introduction

The most prominent experimental results on ICRF heating have been obtained in the combined heating with NBI up to now. Figure 4 shows the

other is (π,0) mode. Phase difference is 180 degrees in toroidal direction and zero in poloidal direction. Typical example of calculation of antenna radiation power spectra for two phasing modes is shown in Fig. 2. The peak position of the spectra is 0 m^{-1} for (0,0) mode and about 10 m^{-1} for (π,0) mode.

Figure 3 shows dependence of the antenna coupling resistance on the line-averaged electron density. The coupling resistance of (0,0) mode is in the range of 4 - 10 Ω and the one of (π,0) mode is 1 - 4 Ω. Previously, we observed large asymmetry of the coupling resistance between upper and lower loops. Recently, we have found that the coupling resistances can be equalized by adjusting the stub tuners. The difference is due to the mutual coupling between the upper and lower loops. The antenna-side stub of the double stub tuners plays an important role in adjusting the mutual coupling. The equalized values are also shown in Fig. 3 by $\ominus$ and $\bullet$ for (0,0) mode and $\circ$ for (π,0) mode. These are located between the previous data of upper and lower loops. Results of the coupling calculation are also shown. Experimental values are in general agreement with the calculated ones.

4. Radiation Loss during ICRF Heating

The radiation loss during ICRF heating has been reduced significantly by replacement of the first wall and the antenna guard limiter with carbon ones. Table 1 compares $\Delta P_{rad}/P_{IC}$, a ratio of the incremental radiation loss associated with ICRF heating to the ICRF power, before and after the replacement.

In the case of TiC wall, $\Delta P_{rad}/P_{IC}$ is dependent on the electron density, phase control and target plasma condition. $\Delta P_{rad}/P_{IC}$ reached about 2 in the low density and ohmic target plasma. This is the worst case. It was reduced with increasing density or injecting neutral beam. After replacement with carbon wall, it has been reduced significantly even in the low density and ohmic target plasma.

5. Beam acceleration during Combined NBI and ICRF Heating

5.1 Introduction

The most prominent experimental results on ICRF heating have been obtained in the combined heating with NBI up to now. Figure 4 shows the

other is (π,0) mode. Phase difference is 180 degrees in toroidal direction and zero in poloidal direction. Typical example of calculation of antenna radiation power spectra for two phasing modes is shown in Fig. 2. The peak position of the spectra is 0 m^{-1} for (0,0) mode and about 10 m^{-1} for (π,0) mode.

Figure 3 shows dependence of the antenna coupling resistance on the line-averaged electron density. The coupling resistance of (0,0) mode is in the range of 4 - 10 Ω and the one of (π,0) mode is 1 - 4 Ω. Previously, we observed large asymmetry of the coupling resistance between upper and lower loops. Recently, we have found that the coupling resistances can be equalized by adjusting the stub tuners. The difference is due to the mutual coupling between the upper and lower loops. The antenna-side stub of the double stub tuners plays an important role in adjusting the mutual coupling. The equalized values are also shown in Fig. 3 by $\ominus$ and $\bullet$ for (0,0) mode and $\circ$ for (π,0) mode. These are located between the previous data of upper and lower loops. Results of the coupling calculation are also shown. Experimental values are in general agreement with the calculated ones.

4. Radiation Loss during ICRF Heating

The radiation loss during ICRF heating has been reduced significantly by replacement of the first wall and the antenna guard limiter with carbon ones. Table 1 compares $\Delta P_{rad}/P_{IC}$, a ratio of the incremental radiation loss associated with ICRF heating to the ICRF power, before and after the replacement.

In the case of TiC wall, $\Delta P_{rad}/P_{IC}$ is dependent on the electron density, phase control and target plasma condition. $\Delta P_{rad}/P_{IC}$ reached about 2 in the low density and ohmic target plasma. This is the worst case. It was reduced with increasing density or injecting neutral beam. After replacement with carbon wall, it has been reduced significantly even in the low density and ohmic target plasma.

5. Beam acceleration during Combined NBI and ICRF Heating

5.1 Introduction

The most prominent experimental results on ICRF heating have been obtained in the combined heating with NBI up to now. Figure 4 shows the

charge exchange (cx) neutral energy spectra. Remarkable beam acceleration was observed during combined NBI and on-axis ICRF heating. Fast ions injected at 60 keV were accelerated up to more than 150 keV.

It was confirmed that the beam acceleration occurs in the plasma core by chopping the neutal beams, whose lines intersects with the line of sights of the cx analyzer in the plasma core. Figure 5 shows the charge exchange spectra. From 6.0 sec to 6.2 sec, injection from the beam lines #9 and #10 were chopped. The high energy tail was not observed in this period as shown in Fig. 5. In this period, however, NBI heating continued from the other beam lines and the beam acceleration should continue. We can conclude that the beam acceleration occurs in the plasma core, since the high energy tail can be observed only when the neutral density in the plasma core on the line of sight of the cx analyzer is enhanced by neutral-injection from the beam lines #9 and #10.

5.2 Parameter Survey[5)]

We examined the dependence of the beam acceleration on the electron density with almost constant NBI and ICRF power. We measure the beam acceleration in ΔT_i^{tail}, which is the difference of the slope of the cx spectra above injection energy between NBI+ICRF and NBI only. Figure 6 shows ΔT_i^{tail} as a function of a slowing-down time, $\tau_s (\propto T_e^{3/2}/n_e)$, which is evaluated from measured $T_e(0)$ and $n_e(0)$. A linear relation $\Delta T_i^{tail} \propto \tau_s$ is confirmed from the experiment. The result is consistent with Fokker-Planck analysis[10)].

Next, we show the dependence on the NBI power with fixed rf power and electron density. ΔT_i^{tail} is almost constant up to P_{NB} of 16 MW as shown in Fig. 7(a). This result implies that the ICRF power density absorbed by the beam component is proportional to P_{NB}. We confirm this by the plot of $n_b \cdot \Delta T_i^{tail}/\tau_s (\propto p_{rf})$ against P_{NB} as shown in Fig. 7(b), where measured cx data at the injection energy is employed for n_b in arbitrary unit. The result is also consistent with the theory[10)].

Efficiency of the beam acceleration is dependent on the phase control of the antenna current. Figure 8 compares ΔT_i^{tail} as a function of P_{IC} between $(\pi,0)$ and $(0,0)$ modes. Efficiency of the beam acceleration of $(\pi,0)$ mode is more than twice as high as the one of $(0,0)$ mode.

5.3 Beam Acceleration under Optimized Conditions[11)]

Experimental result on the beam acceleration under optimized conditions, which were clarified by the parameter survey described in section 5.2, is shown in Fig. 9 by solid lines (shot E5764). The dotted lines (E5795) are added to make clear the baseline of the shot E5764.

The plasma stored energy increased from the ohmic level by 1.2 MJ with NBI of 18 MW and further increased by 0.3 MJ with ICRF of only 1.4 MW. It should be noted that the plasma stored energy did not saturate during the pulse length of ICRF, although the electron density continued to decrease during the ICRF pulse.

The number of energetic ions whose energy is higher than the injection energy (70 keV) increased significantly with ICRF heating, but that less than the injection energy changed little with ICRF heating, indicating that the beam acceleration occurred. The electron temperature in the center and the sawteeth period were also enhanced with increasing population of the energetic ions.

The incremental energy confinement time of NBI in the NBI heating alone phase is 70 msec, while the one of ICRF during combined heating is 210 msec. Thus, strong synergetic effect was observed during combined heating.

The charge exchange energy spectra of the shot E5764 are shown in Fig. 10. Data of the NBI heating at t=4.9 sec are shown by open squares and those of the combined heating at t=5.9 sec by closed circles. The broken line is the fitting by the Fokker-Planck calculation.[10)] We thus evaluate the ICRF power density as 0.34 MW/m^3 from the fitting analysis. A ratio of the beam ion density to the total ion density amounts to 18% during the NBI heating only. It increases up to 40% during the combined heating. Thus, the beam ions occupy a significant population in the total ion density during the combined heating. Therefore, we evaluate ion average energy as an effective ion temperature in the form,

$$T_i^{eff} = \frac{2}{3}\int_0^\infty \frac{1}{2} M\upsilon^2 F_0(\upsilon)\upsilon^2 d\upsilon \Big/ \int_0^\infty F_0(\upsilon)\upsilon^2 d\upsilon \ , \qquad (1)$$

where F_0, M and v are the isotropic ion velocity distribution determined by the fitting, the mass and the velocity of an ion, respectively. T_i^{eff} increases from 12 keV during NBI heating only up to 22 keV during the combined heating in the shot E5764.

Figure 11 compares the power deposition profiles between NBI and ICRF.

We determine the radius of the ICRF power deposition from the power density obtained by the fitting analysis of the cx spectra and the torus input power. Those of NBI is from Monte-Carlo code. In this case, the power density of ICRF, p_{IC}, is more than 50% of that of NBI, $p_{be}+p_{bi}$, in the plasma center, although the torus input of ICRF is by an order of magnitude less than that of NBI. ICRF heating is thus efficient for central heating.

A self consistent code which incorporates a global wave structure and a quasi-linear velocity diffusion has been developed[12,13]. A comparative analysis between the experiment and the calculation is being in progress.

5.4 Enhancemant of τ_E^{inc} with Beam Acceleration[11]

Figure 12 summarizes incremental energy confinement time, τ_E^{inc} ($\equiv \Delta W/\Delta P$; ΔW is incremental stored energy due to additional heating power ΔP) against $\bar{n}_e$ for various heating methods. Open simbols show τ_E^{inc} of ICRF during combined NBI and ICRF heating and closed ones indicate ICRF heating alone case. Circles indicate B_T = 4 T case (on-axis heating) and triangles B_T = 4.5 T case (off-axis heating). The broken line is τ_E^{inc} of NBI heating alone. τ_E^{inc} in excess of 200 msec is obtained for ICRF during combined heating, which is about three times as long as that of NBI only or ICRF only case. However, τ_E^{inc} decreases with increasing electron density, since beam acceleration becomes less dominant with increasing electron density.

A simple scaling of the incremental energy confinement time of ICRF during combined NBI and ICRF heating is written as

$$\tau_E^{inc} = \eta_b \cdot \tau_s + \tau_{E0}^{inc} \qquad (2)$$

where η_b is a ratio of the ICRF power absorbed by the beam ions to the total ICRF power, τ_s is the ion-electron energy relaxation time and τ_{E0}^{inc} is the incremental energy confinement time of the bulk plasma. Equation (2) is derived from a steady-state power balance of the two-components plasma. η_b is calculated from the scaling of the rf power density deposited on the ions having the non-Maxwellian beam-induced and rf-induced tail[10].

The experimental data are plotted as a function of $\eta_b \cdot \tau_s$ as shown in Fig. 13. We confirm that the scaling fits the experimental data very well. Therefore, we can conclude that the beam ions accelerated by the ICRF wave behave classically, although the bulk plasma follows typical L-mode

scaling. It is important from point of view of the plasma confinement to inject more ICRF power and to investigate the behaviour of the high energy ions which dominate the total ion population.

6. ICRF Heating of OH Plasma

The second harmonic ICRF heating is also effective for ohmic plasma in the case of $(\pi,0)$ phasing. Figure 14 shows time evolution of P_{IC} and the electron temperature measured by filter method of soft X-ray for (a) on-axis heating and (b) off-axis heating. The cyclotron resonance layer is about 40 cm outside from the axis in the latter case.

The central electron temperature and the sawteeth period are enhanced with on-axis ICRF heating. Peaked profile of the electron temperature is obtained with on-axis heating.

7. Antenna-Plasma Coupling during H-mode[14)]

H-mode phenomena were observed during combined NBI and ICRF heating in JT-60. H-transition was seen both in $(\pi,0)$ and (0,0) modes. Figure 15 shows time evolution of the antenna coupling resistance, the line-integral electron density, H_α signal, the plasma stored energy measured by diamagnetic loop, NBI power and ICRF power for (a) $(\pi,0)$ mode and (b) (0,0) mode. Period of H-mode is indicated by two vertical broken lines in each figure. At the H-transition, H_α signal was depressed and the electron density and the plasma stored energy increased in both cases. The antenna coupling resistance, however, showed different response between both phasing modes, i.e. the antenna coupling resistance increased at the H-transition in $(\pi,0)$ mode, while it decreased in (0,0) mode.

A reduction of the antenna coupling resistance during H-mode has been observed in other tokamaks. In JT-60, however, the coupling resistance of $(\pi,0)$ mode has been found to increase during H-mode transition, although the one of (0,0) mode decreases.

This is explained with the antenna-plasma coupling code taking into account the change of the electron density profile. Figure 16 shows electron density profiles of L-mode and H-mode. Broken lines indicate cut-off density of fast wave for various values of $k_\parallel$. The cut-off surface for large $k_\parallel$ ($> 10\ m^{-1}$) exists inside the separatrix. Therefore, it becomes close to the antenna after H-transition. This is the reason why the

scaling. It is important from point of view of the plasma confinement to inject more ICRF power and to investigate the behaviour of the high energy ions which dominate the total ion population.

6. ICRF Heating of OH Plasma

The second harmonic ICRF heating is also effective for ohmic plasma in the case of $(\pi,0)$ phasing. Figure 14 shows time evolution of P_{IC} and the electron temperature measured by filter method of soft X-ray for (a) on-axis heating and (b) off-axis heating. The cyclotron resonance layer is about 40 cm outside from the axis in the latter case.

The central electron temperature and the sawteeth period are enhanced with on-axis ICRF heating. Peaked profile of the electron temperature is obtained with on-axis heating.

7. Antenna-Plasma Coupling during H-mode[14)]

H-mode phenomena were observed during combined NBI and ICRF heating in JT-60. H-transition was seen both in $(\pi,0)$ and $(0,0)$ modes. Figure 15 shows time evolution of the antenna coupling resistance, the line-integral electron density, H_α signal, the plasma stored energy measured by diamagnetic loop, NBI power and ICRF power for (a) $(\pi,0)$ mode and (b) $(0,0)$ mode. Period of H-mode is indicated by two vertical broken lines in each figure. At the H-transition, H_α signal was depressed and the electron density and the plasma stored energy increased in both cases. The antenna coupling resistance, however, showed different response between both phasing modes, i.e. the antenna coupling resistance increased at the H-transition in $(\pi,0)$ mode, while it decreased in $(0,0)$ mode.

A reduction of the antenna coupling resistance during H-mode has been observed in other tokamaks. In JT-60, however, the coupling resistance of $(\pi,0)$ mode has been found to increase during H-mode transition, although the one of $(0,0)$ mode decreases.

This is explained with the antenna-plasma coupling code taking into account the change of the electron density profile. Figure 16 shows electron density profiles of L-mode and H-mode. Broken lines indicate cut-off density of fast wave for various values of $k_\parallel$. The cut-off surface for large $k_\parallel$ ($> 10\ m^{-1}$) exists inside the separatrix. Therefore, it becomes close to the antenna after H-transition. This is the reason why the

scaling. It is important from point of view of the plasma confinement to inject more ICRF power and to investigate the behaviour of the high energy ions which dominate the total ion population.

6. ICRF Heating of OH Plasma

The second harmonic ICRF heating is also effective for ohmic plasma in the case of $(\pi,0)$ phasing. Figure 14 shows time evolution of P_{IC} and the electron temperature measured by filter method of soft X-ray for (a) on-axis heating and (b) off-axis heating. The cyclotron resonance layer is about 40 cm outside from the axis in the latter case.

The central electron temperature and the sawteeth period are enhanced with on-axis ICRF heating. Peaked profile of the electron temperature is obtained with on-axis heating.

7. Antenna-Plasma Coupling during H-mode[14)]

H-mode phenomena were observed during combined NBI and ICRF heating in JT-60. H-transition was seen both in $(\pi,0)$ and (0,0) modes. Figure 15 shows time evolution of the antenna coupling resistance, the line-integral electron density, H_α signal, the plasma stored energy measured by diamagnetic loop, NBI power and ICRF power for (a) $(\pi,0)$ mode and (b) (0,0) mode. Period of H-mode is indicated by two vertical broken lines in each figure. At the H-transition, H_α signal was depressed and the electron density and the plasma stored energy increased in both cases. The antenna coupling resistance, however, showed different response between both phasing modes, i.e. the antenna coupling resistance increased at the H-transition in $(\pi,0)$ mode, while it decreased in (0,0) mode.

A reduction of the antenna coupling resistance during H-mode has been observed in other tokamaks. In JT-60, however, the coupling resistance of $(\pi,0)$ mode has been found to increase during H-mode transition, although the one of (0,0) mode decreases.

This is explained with the antenna-plasma coupling code taking into account the change of the electron density profile. Figure 16 shows electron density profiles of L-mode and H-mode. Broken lines indicate cut-off density of fast wave for various values of $k_\parallel$. The cut-off surface for large $k_\parallel$ ($> 10\ m^{-1}$) exists inside the separatrix. Therefore, it becomes close to the antenna after H-transition. This is the reason why the

coupling resistance increased during H-mode for $(\pi,0)$ mode.

8. Summary

(1) During the combined heating of NBI and ICRF, the remarkable beam acceleration was observed and the plasma stored energy increased very efficiently. This improvement of the energy confinement is explained as the build-up of the fast ions accelerated by ICRF.

(2) H-mode phenomena were observed during combined NBI and ICRF heating in many shots. It is demonstrated that such large $k_{\parallel}$ excitation as $(\pi,0)$ mode improves the antenna coupling during H-mode.

(3) Peaked electron temperature profile was obtained with on-axis ICRF heating.

(4) Radiation loss during ICRF heating has been reduced significantly with carbon first wall and carbon guard limiter of the antenna.

9. Experimental Programme in 1988

The frequency has been changed from 120 MHz to 131 MHz in March, 1988 in order to match the frequency to the full toroidal magnetic field of JT-60, i.e. 4.8 T. The ICRF experimental programme for the next experimental period is as follows.

(1) Enhancement of $n_e(0)\tau_E T_i(0)$ with
on-axis ICRF heating ($\gtrsim$ 3 MW),
intense NBI heating ($\sim$ 25 MW),
high plasma current ($\lesssim$ 3.5 MA) and
pellet fueling.

(2) Expansion of the database of ICRF heating alone with phase control, pellet, etc.

(3) H-mode study with combined NBI and ICRF heating in the lower single null divertor configuration.

(4) Fast wave current drive experiment with assistance of LHRF.

coupling resistance increased during H-mode for $(\pi,0)$ mode.

8. Summary

(1) During the combined heating of NBI and ICRF, the remarkable beam acceleration was observed and the plasma stored energy increased very efficiently. This improvement of the energy confinement is explained as the build-up of the fast ions accelerated by ICRF.

(2) H-mode phenomena were observed during combined NBI and ICRF heating in many shots. It is demonstrated that such large $k_{\parallel}$ excitation as $(\pi,0)$ mode improves the antenna coupling during H-mode.

(3) Peaked electron temperature profile was obtained with on-axis ICRF heating.

(4) Radiation loss during ICRF heating has been reduced significantly with carbon first wall and carbon guard limiter of the antenna.

9. Experimental Programme in 1988

The frequency has been changed from 120 MHz to 131 MHz in March, 1988 in order to match the frequency to the full toroidal magnetic field of JT-60, i.e. 4.8 T. The ICRF experimental programme for the next experimental period is as follows.

(1) Enhancement of $n_e(0)\tau_E T_i(0)$ with
on-axis ICRF heating ($\gtrsim$ 3 MW),
intense NBI heating ($\sim$ 25 MW),
high plasma current ($\lesssim$ 3.5 MA) and
pellet fueling.

(2) Expansion of the database of ICRF heating alone with phase control, pellet, etc.

(3) H-mode study with combined NBI and ICRF heating in the lower single null divertor configuration.

(4) Fast wave current drive experiment with assistance of LHRF.

coupling resistance increased during H-mode for $(\pi,0)$ mode.

8. Summary

(1) During the combined heating of NBI and ICRF, the remarkable beam acceleration was observed and the plasma stored energy increased very efficiently. This improvement of the energy confinement is explained as the build-up of the fast ions accelerated by ICRF.

(2) H-mode phenomena were observed during combined NBI and ICRF heating in many shots. It is demonstrated that such large $k_{\parallel}$ excitation as $(\pi,0)$ mode improves the antenna coupling during H-mode.

(3) Peaked electron temperature profile was obtained with on-axis ICRF heating.

(4) Radiation loss during ICRF heating has been reduced significantly with carbon first wall and carbon guard limiter of the antenna.

9. Experimental Programme in 1988

The frequency has been changed from 120 MHz to 131 MHz in March, 1988 in order to match the frequency to the full toroidal magnetic field of JT-60, i.e. 4.8 T. The ICRF experimental programme for the next experimental period is as follows.

(1) Enhancement of $n_e(0)\tau_E T_i(0)$ with
on-axis ICRF heating ($\gtrsim$ 3 MW),
intense NBI heating ($\sim$ 25 MW),
high plasma current ($\lesssim$ 3.5 MA) and
pellet fueling.

(2) Expansion of the database of ICRF heating alone with phase control, pellet, etc.

(3) H-mode study with combined NBI and ICRF heating in the lower single null divertor configuration.

(4) Fast wave current drive experiment with assistance of LHRF.

10. Future Plan

Upgrade of the ICRF heating system is considered for JT-60U (D-shaped, lower-side divertor, 6 MA) as follows.

(1) 1990 ~ 1992

Generator output ; 12 MW
by replacement of the tetrode 8973 with X-2242
Frequency range ; 108 MHz ~ 132 MHz (unchanged)
Antenna ; phased loop array
Number of antenna ; 2

(2) 1993 ~

Main experimental programme in this stage is current drive experiment in the high electron density regime. Current driver for this experiment will be determined in near future. ICRF is considered as one of the possible methods for the high density current drive experiment.

Tentative specification:

Torus input ; 24 MW
Frequency range ; 40 MHz ~ 130 MHz

Acknowledgement

We are much indebted to Drs. M. Yamagiwa and T. Takizuka for Fokker-Planck calculation and valuable discussion. We would also like to thank Drs. M. Yoshikawa, K. Tomabechi and S. Mori for their encouragement.

10. Future Plan

Upgrade of the ICRF heating system is considered for JT-60U (D-shaped, lower-side divertor, 6 MA) as follows.

(1) 1990 ~ 1992

Generator output ; 12 MW
by replacement of the tetrode 8973 with X-2242
Frequency range ; 108 MHz ~ 132 MHz (unchanged)
Antenna ; phased loop array
Number of antenna ; 2

(2) 1993 ~

Main experimental programme in this stage is current drive experiment in the high electron density regime. Current driver for this experiment will be determined in near future. ICRF is considered as one of the possible methods for the high density current drive experiment.

Tentative specification:

Torus input ; 24 MW
Frequency range ; 40 MHz ~ 130 MHz

Acknowledgement

We are much indebted to Drs. M. Yamagiwa and T. Takizuka for Fokker-Planck calculation and valuable discussion. We would also like to thank Drs. M. Yoshikawa, K. Tomabechi and S. Mori for their encouragement.

References

1) M. Yoshikawa, et al., in Proceedings of the 11th Int. Conf. on Plasma Physics and Controlled Nuclear Fusion Research, Kyoto, 1986, (International Atomic Energy Agency, Vienna, 1987), Vol.1, 11.
2) T. Nagashima, et al., Fusion Engineering and Design 5 (1987) 101.
3) M. Saigusa, et al., in Proceedings of 7th Topical Conference on Application of Radio-Frequency Power to Plasmas, Kissimmee, Florida, 1987.
4) K. Hamamatsu, et al., Jpn. J. Appl. Phys., 26 (1987) 1525.
5) H. Kimura, et al., in Proceedings of 14th European Conference on Controlled Fusion and Plasma Physics, Madrid, Spain, 1987, (European Physical Society, 1987), Vol.11D, Pt.3, 857.
6) K. Steinmetz, invited paper in Ref. 3.
7) T. Fujii, et al., in Proceedings of 15th European Conference on Controlled Fusion and Plasma Physics, Dubrovnik, 1988, (European Physical Society, 1988), Vol.12B. Pt.2, 766.
8) H. Kimura, et al., in Proceedings of 12th Symp. on Fusion Engineering, Montrey, 1987.
9) K. Sakamoto, et al., in Proceedings of 11th Symp. on Fusion Engineering, Austin, 1985, Vol.2, 1196.
10) M. Yamagiwa, et al., Japan Atomic Energy Research Institute Report JAERI-M 87-127 (1987); to be published in Plasma Phys. Controlled Fusion.
11) H. Kimura, et al., submitted to Phys. Rev. Lett.
12) K. Hamamatsu, et al., in Ref. 4, P861.
13) K. Hamamatsu, et al., Institute for Fusion Theory, Hiroshima University, Report HIFT-151 (1988).
14) M. Saigusa, et al., submitted to Nucl. Fusion.

Table 1 Ratio of incremental radiation loss associated with ICRF heating to ICRF power for various conditions.

TiC Wall (September, 1986 ~ March, 1987)

	OH+ICRF		OH+NBI+ICRF
$\bar{n}_e$ ($10^{19}m^{-3}$)	~4	~6	3~4
$\Delta P_{rad}/P_{IC}$; (0,0)	2.2	1	0.5
$\Delta P_{rad}/P_{IC}$; (π,0)	1.8	0.65	0.8

Carbon Wall (since July, 1987)

	OH+ICRF	OH+NBI+ICRF
$\bar{n}_e$ ($10^{19}m^{-3}$)	2.1~3.5	2.1~3.5
$\Delta P_{rad}/P_{IC}$; (π,0)	0.2	0.3

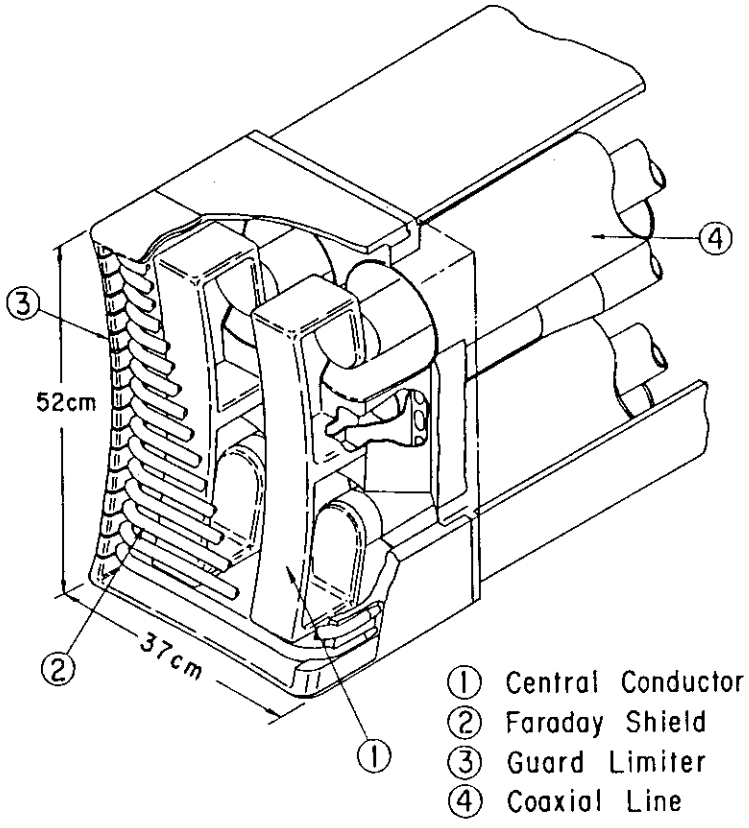

Fig. 1 Structure of the 2×2 phased loop antenna array of JT-60.

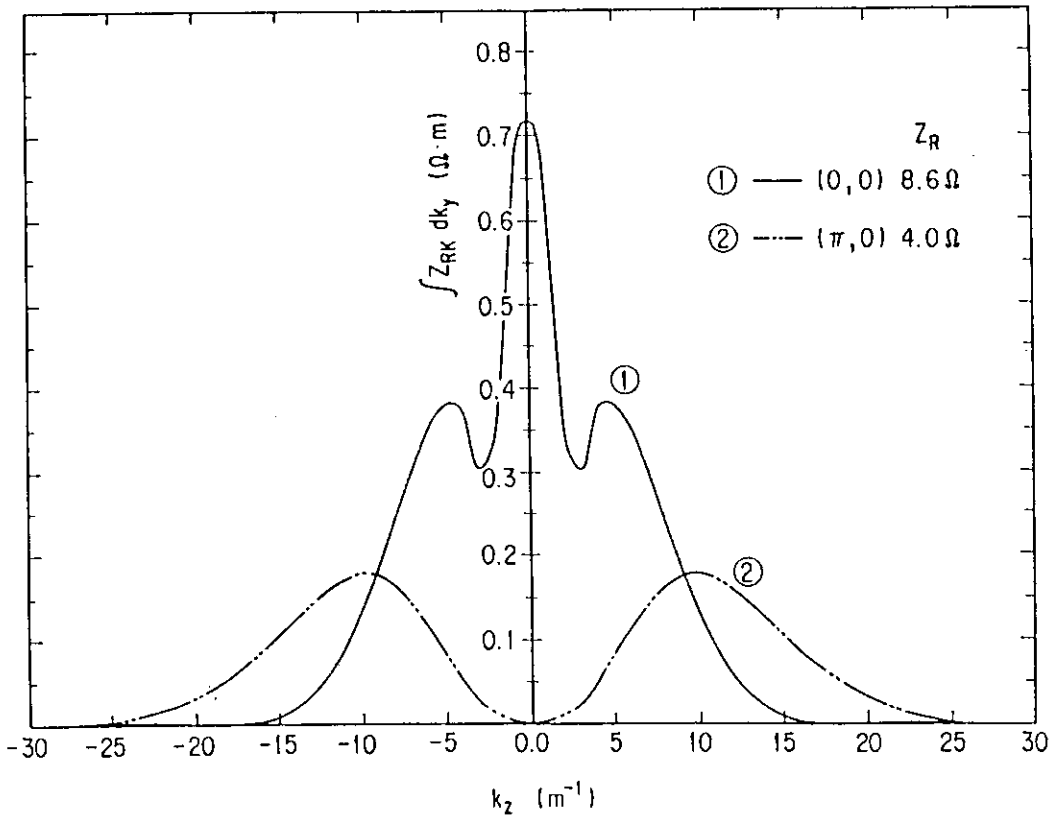

Fig. 2 Radiation power spectra of the 2×2 loop antenna.

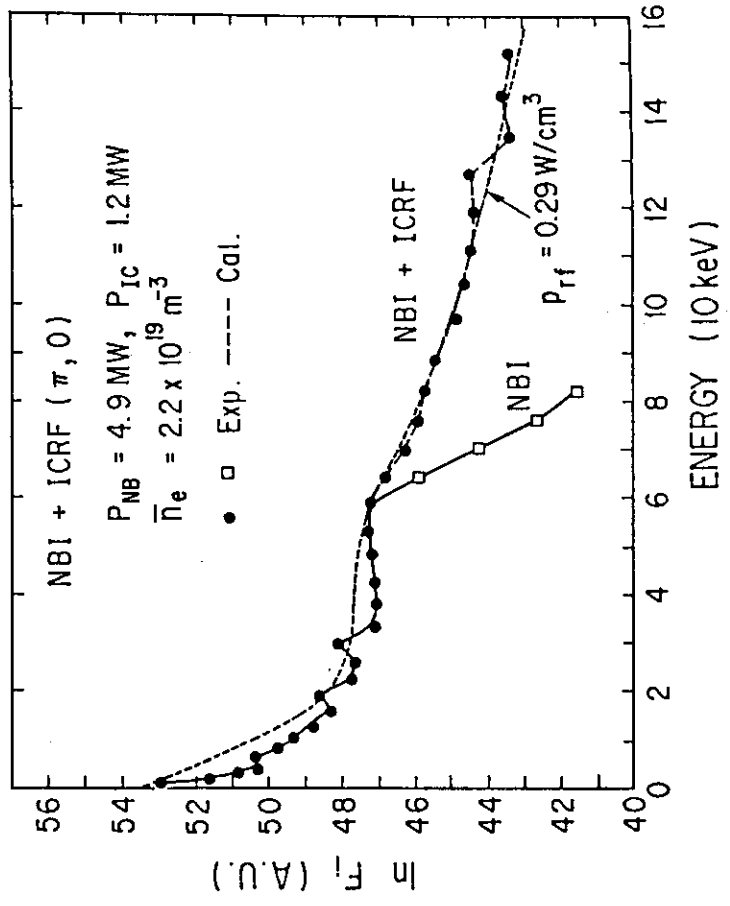

Fig. 4 Charge exchange neutral energy spectra during combined NBI and ICRF heating and NBI heating alone. The broken line is fitting by the Fokker-Planck calculation. I_p=1.5 MA, B_T=4 T, divertor discharge.

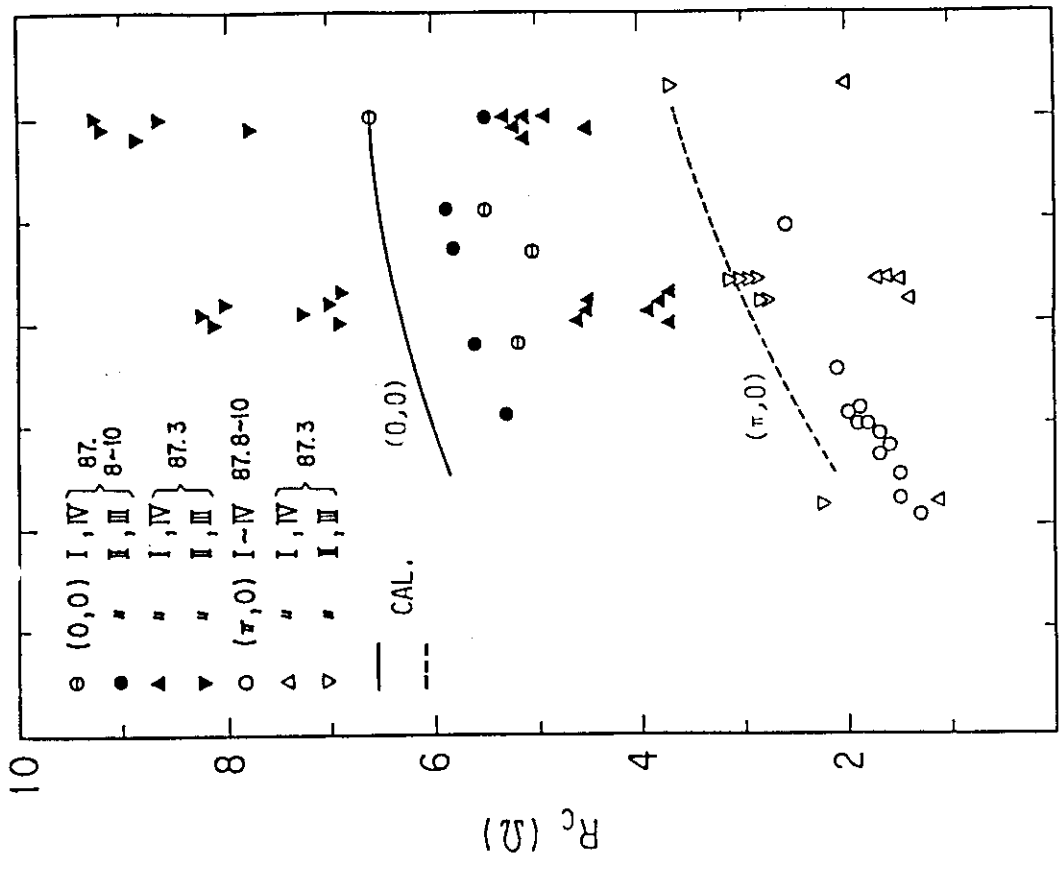

Fig. 3 Dependence of antenna coupling resistance on line-averaged electron density.

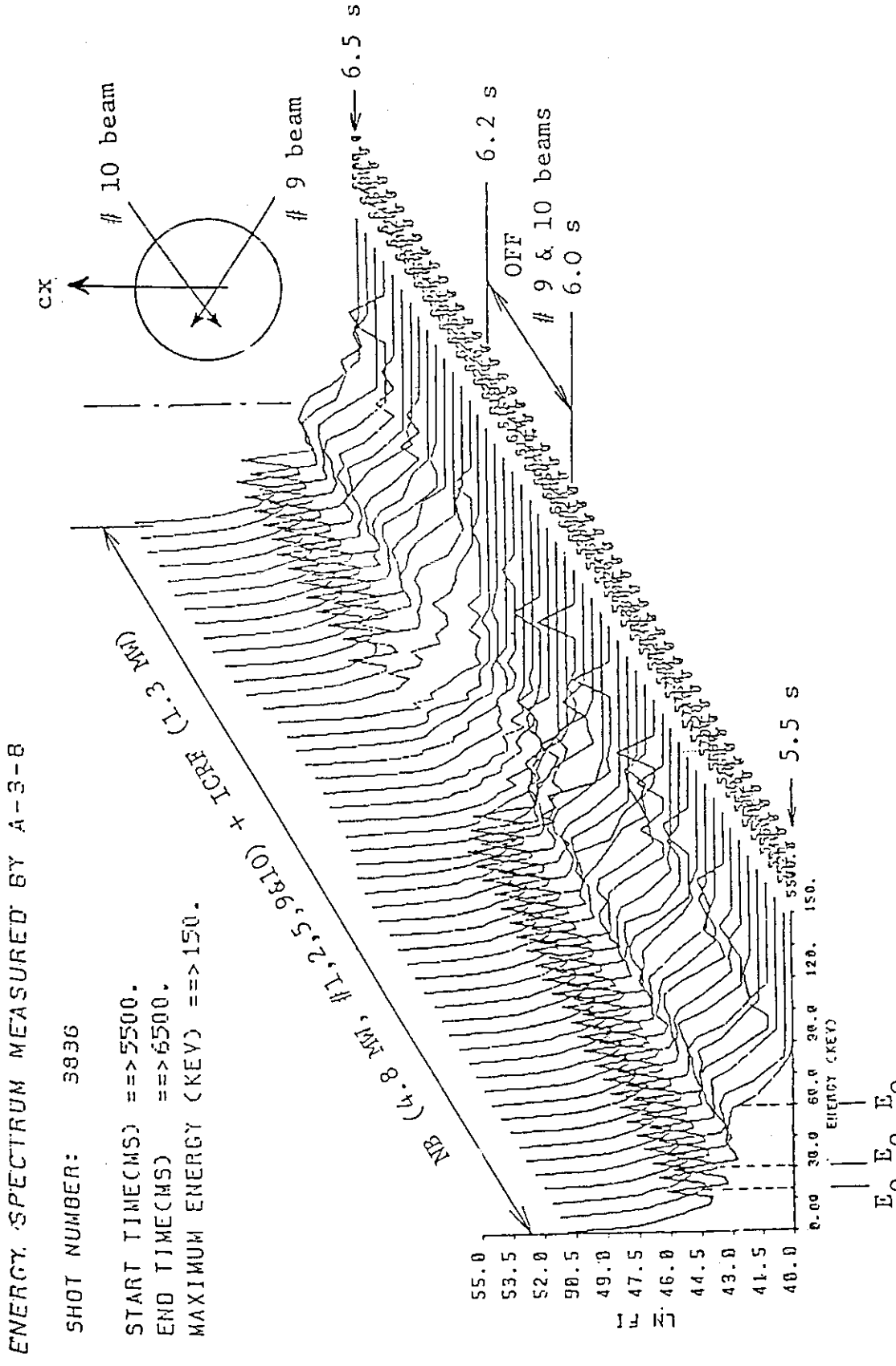

Fig. 5 Time evolution of charge exchange neutral energy spectra. I_p=1.5 MA, B_T=4 T, divertor discharge, $\bar{n}_e$=6.3×10^{19} m^{-3}. ICRF; (0,0) mode.

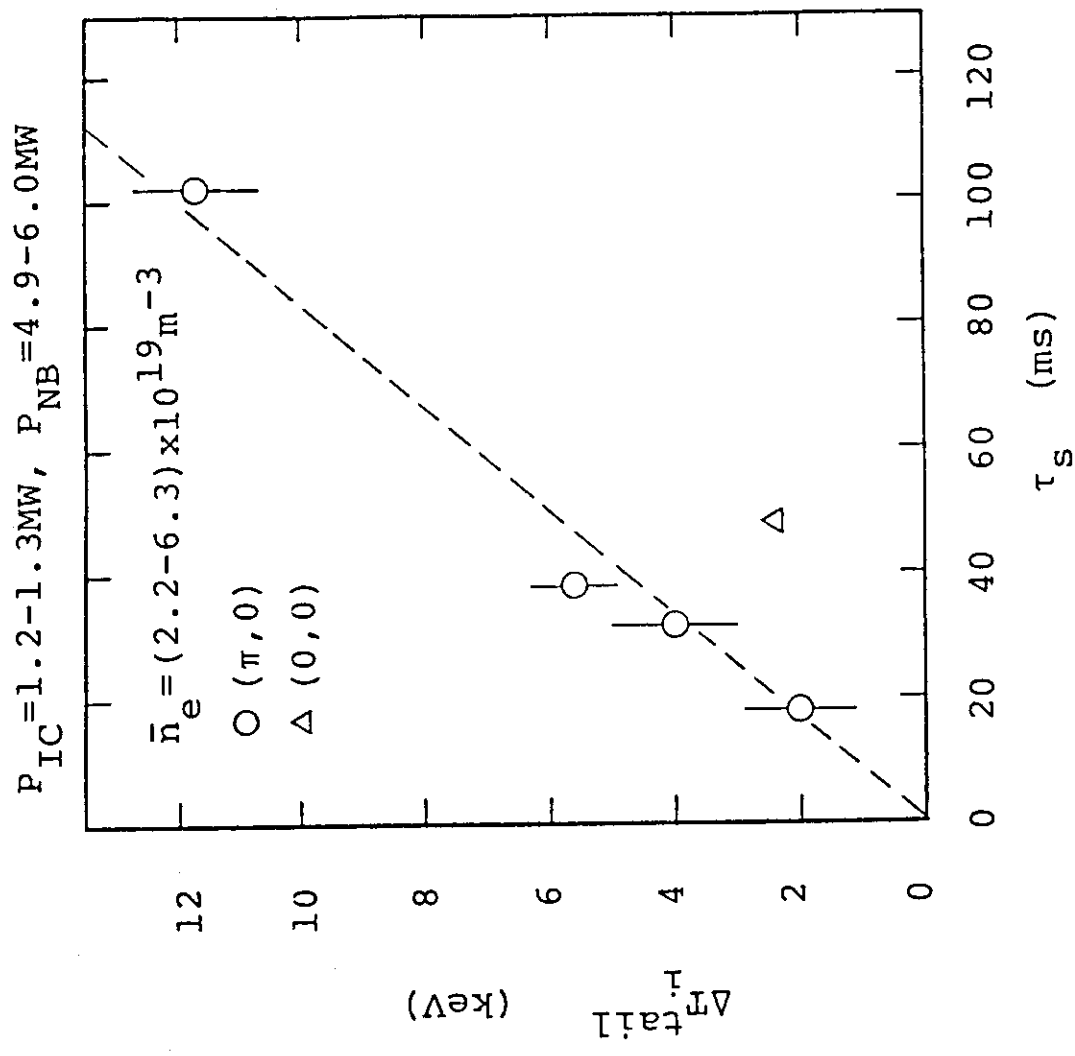

Fig. 6 ΔT_i^{tail} against τ_s (n_e-scan). I_p=1.5 MA, B_T=4 T, divertor discharge.

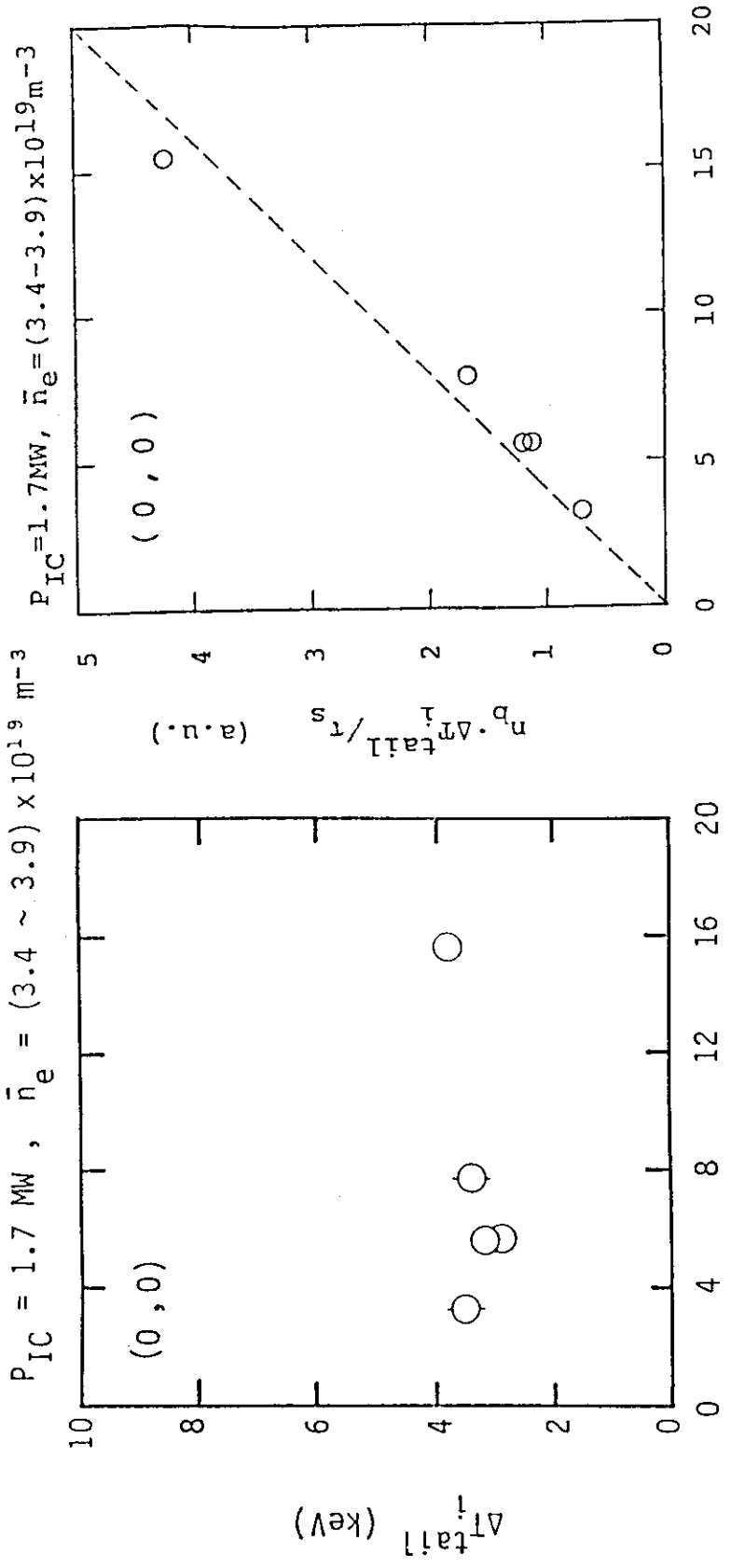

Fig. 7 (a) ΔT_i^{tail} against P_{NB}. I_p=1.5 MA, B_T=4 T, divertor discharge.
(b) $n_b \cdot \Delta_i^{tail}/\tau_s$ against P_{NB}. The same conditions as in (a).

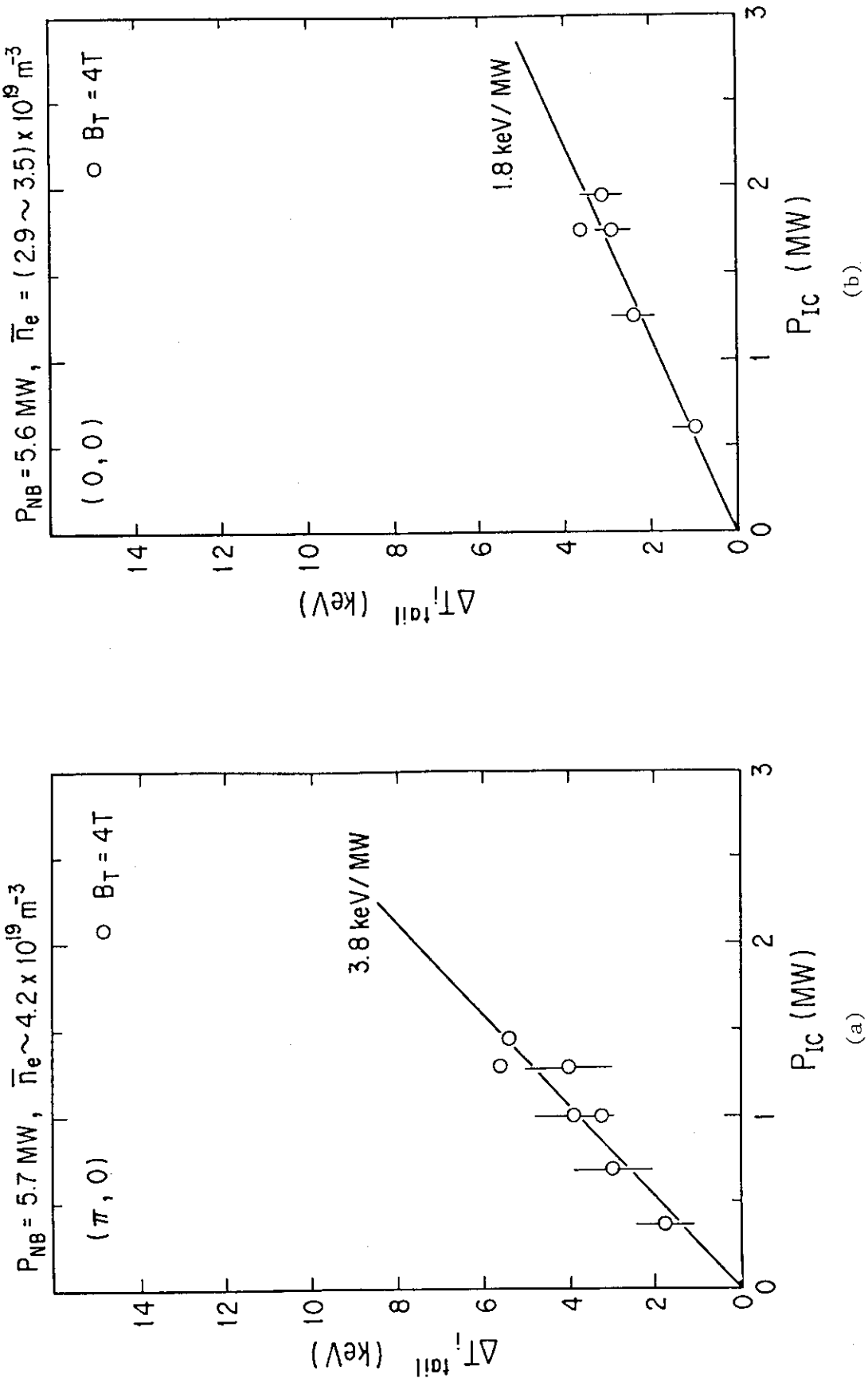

Fig. 8 ΔT_i^{tail} against P_{IC}. (a) (π,0) mode, (b) (0,0) mode.
I_p=1.5 MA, B_T=4 T, divertor discharge.

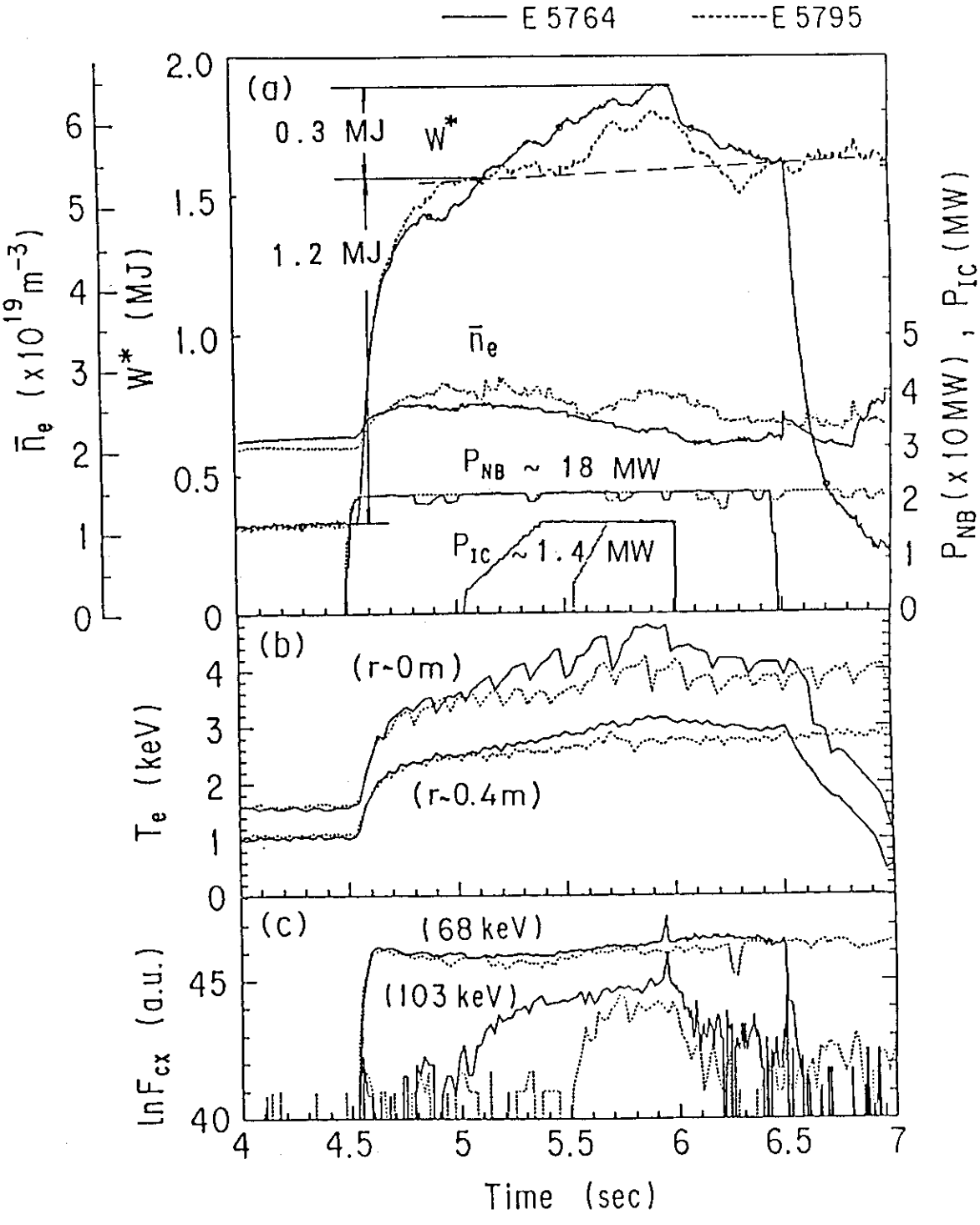

Fig. 9 Time evolutions of (a) plasma stored energy, line-averaged electron density, NBI power (torus input), ICRF power (antenna radiation power including circuit loss), (b) electron temperature at the plasma center and r ~ 0.4 m and (c) charge exchange neutral fluxes at the NBI injection energy (68 keV) and above the injection energy (103 keV) for the shot E5764 (solid lines). Dotted lines (shot E5795) are included for comparison. I_p=1.5 MA, B_T=4 T, P_{NB} (absorbed power) = 18 MW and P_{IC} (antenna radiation power excluding circuit loss) = 1.4 MW.

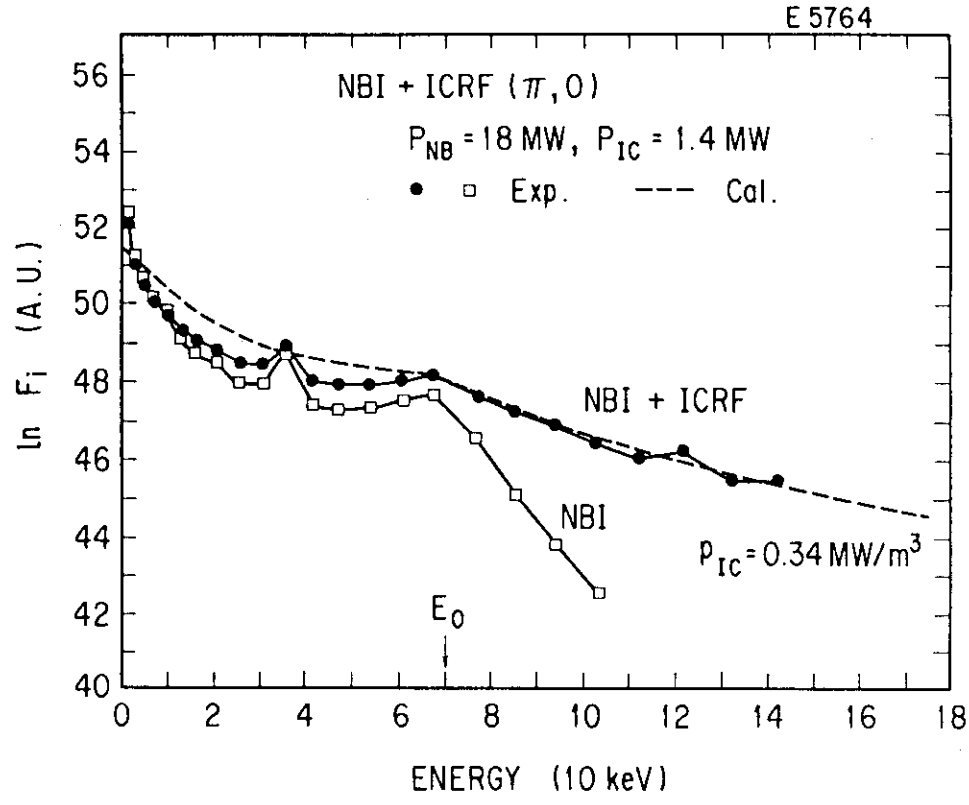

Fig. 10 Charge exchange energy spectra of the shot E5764 during the combined heating (t=5.9 sec) and NBI alone (t=4.9 sec). The result of the Fokker-Planck calculation is also shown (broken line).

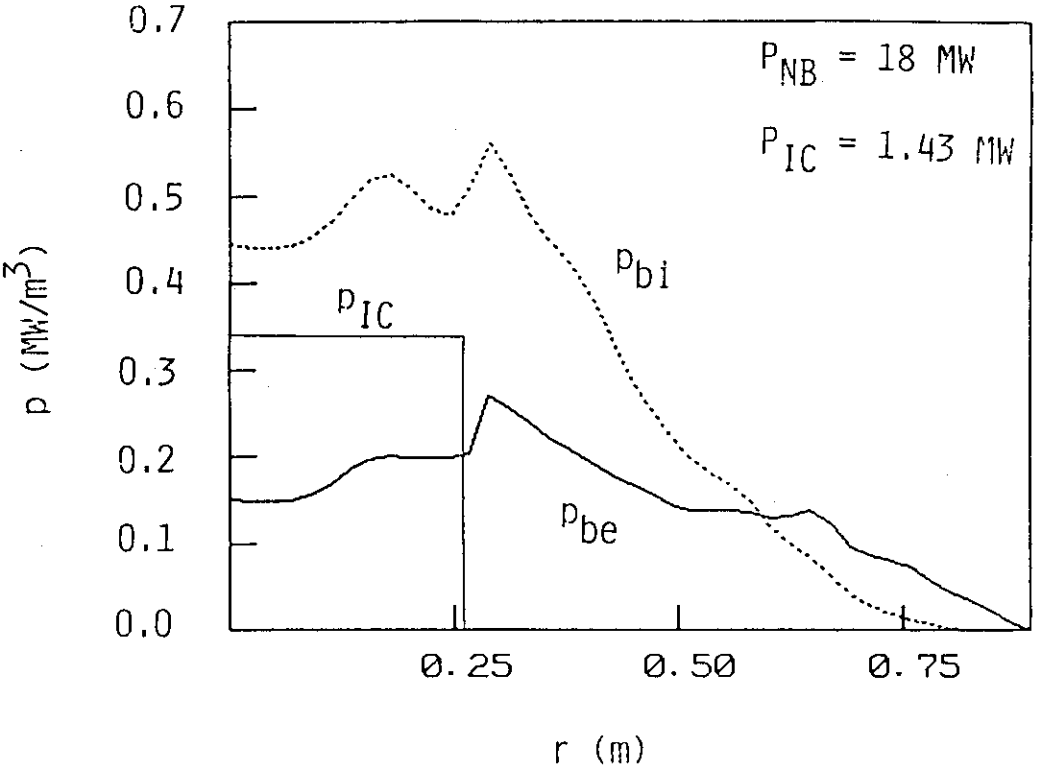

Fig. 11 Comparison of power deposition profiles between NBI and ICRF.

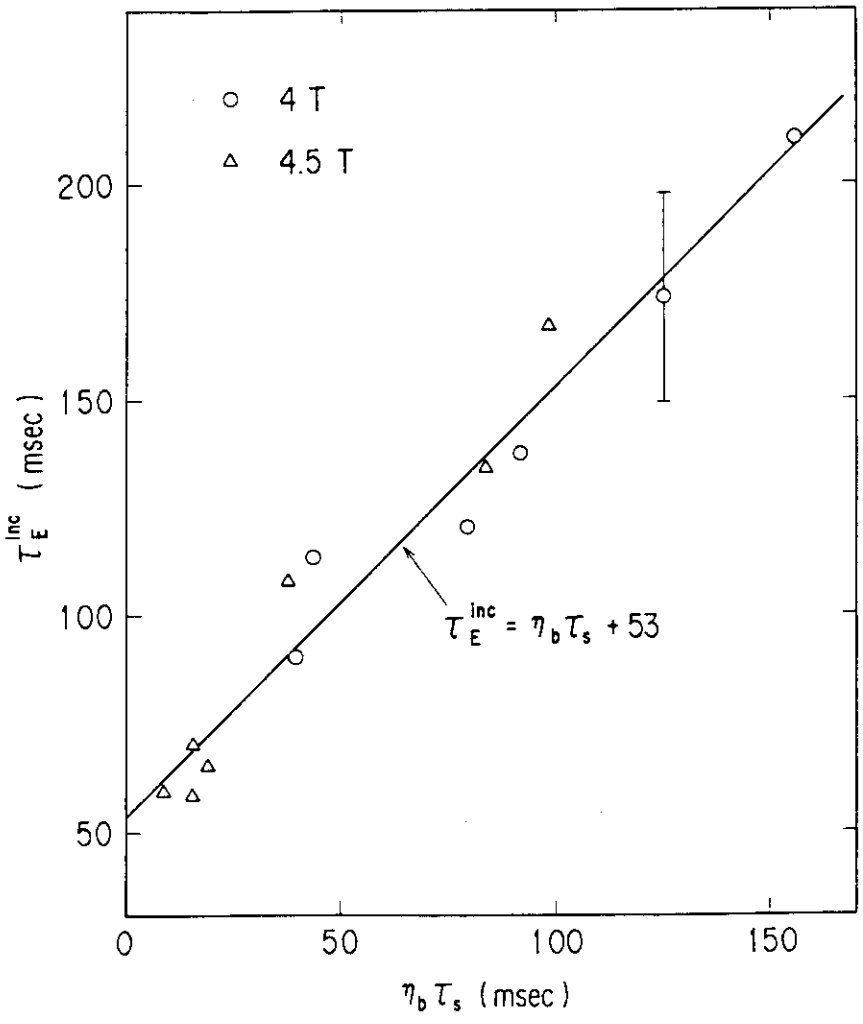

Fig. 12 Incremental energy confinement time τ_E^{inc} against line-averaged electron density $\bar{n}_e$. Open circles and triangles are those corresponding to the ICRF heating during the combined heating for B_T of 4 T (on-axis heating) and 4.5 T (off-axis heating), respectively. Those of ICRF alone are indicated with closed circles and triangles. Broken line shows the level of NBI heating alone.

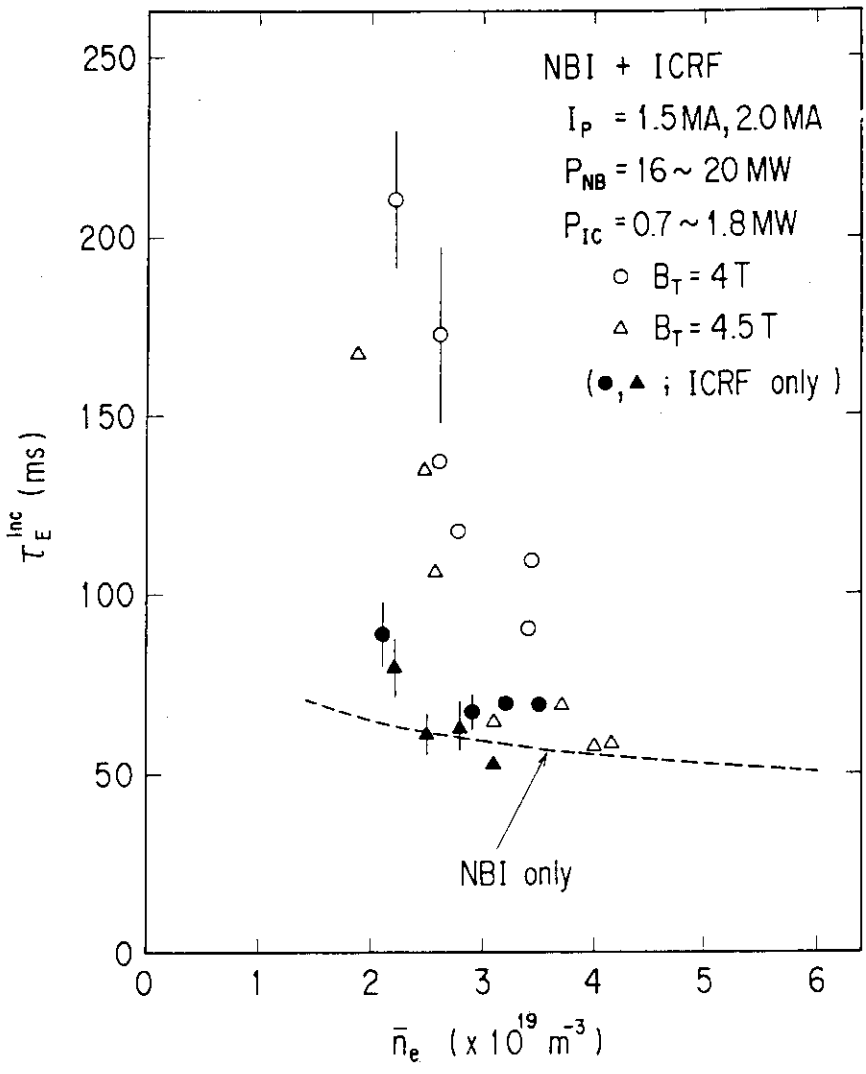

Fig. 13 Incremental energy confinement time τ_E^{inc} for ICRF during the combined heating as a function of $n_b \cdot \tau_s$ for B_T=4 T (circles) and 4.5 T (triangles). The result of linear-regression analysis is shown by solid line.

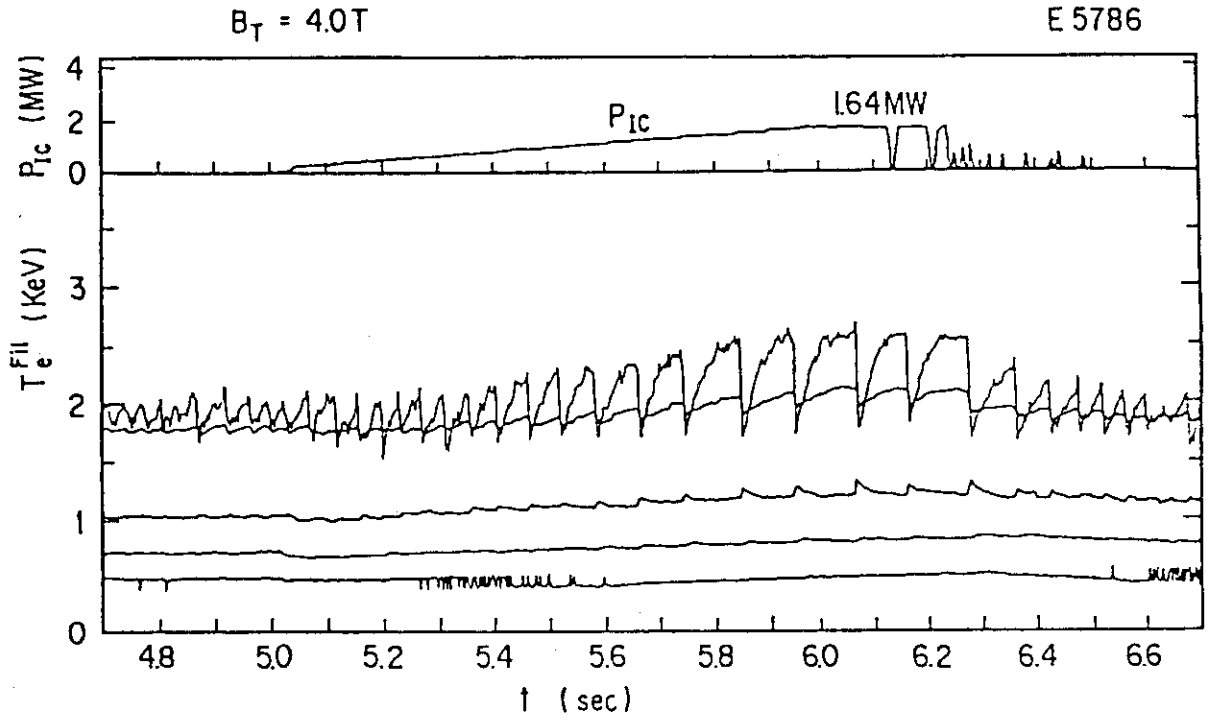

(a)

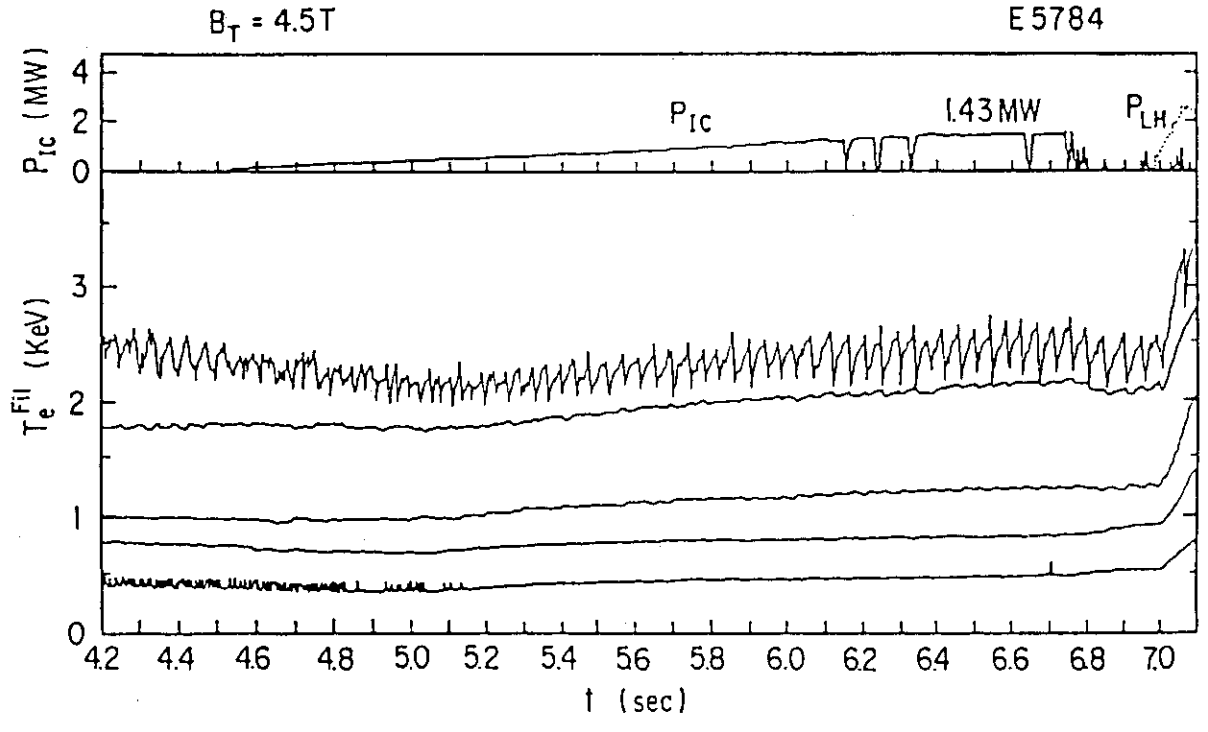

(b)

Fig. 14 Time evolution of ICRF power and the electron temperature from soft X-ray filter method at various positions. $T_e^{Fil}(r)$; r=0, 0.2, 0.4, 0.6, 0.8 m from the top. (a) on-axis heating, (b) off-axis heating. I_p=1.5 MA, divertor discharge. ICRF; (π,0) mode.

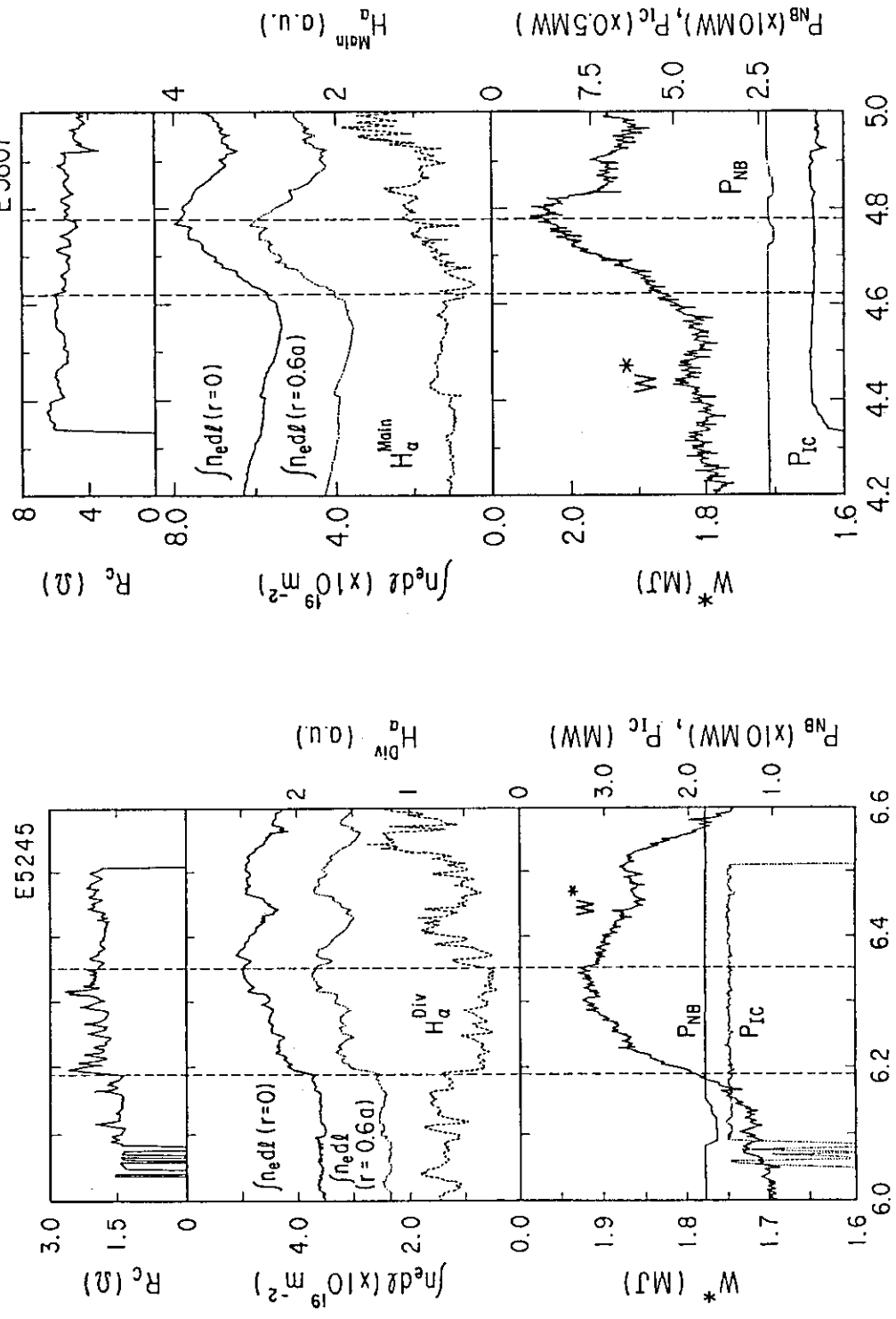

Fig. 15 Time evolution of antenna coupling resistance, line-integral electron density, H_α signal, plasma stored energy, NBI power and ICRF power. (a) (π,0) mode, I_p=2 MA, B_T=4.5 T, divertor discharge, (b) (0,0) mode, I_p=2.7 MA, B_T=4.8 T, divertor discharge. The period between the two broken lines indicate H-mode.

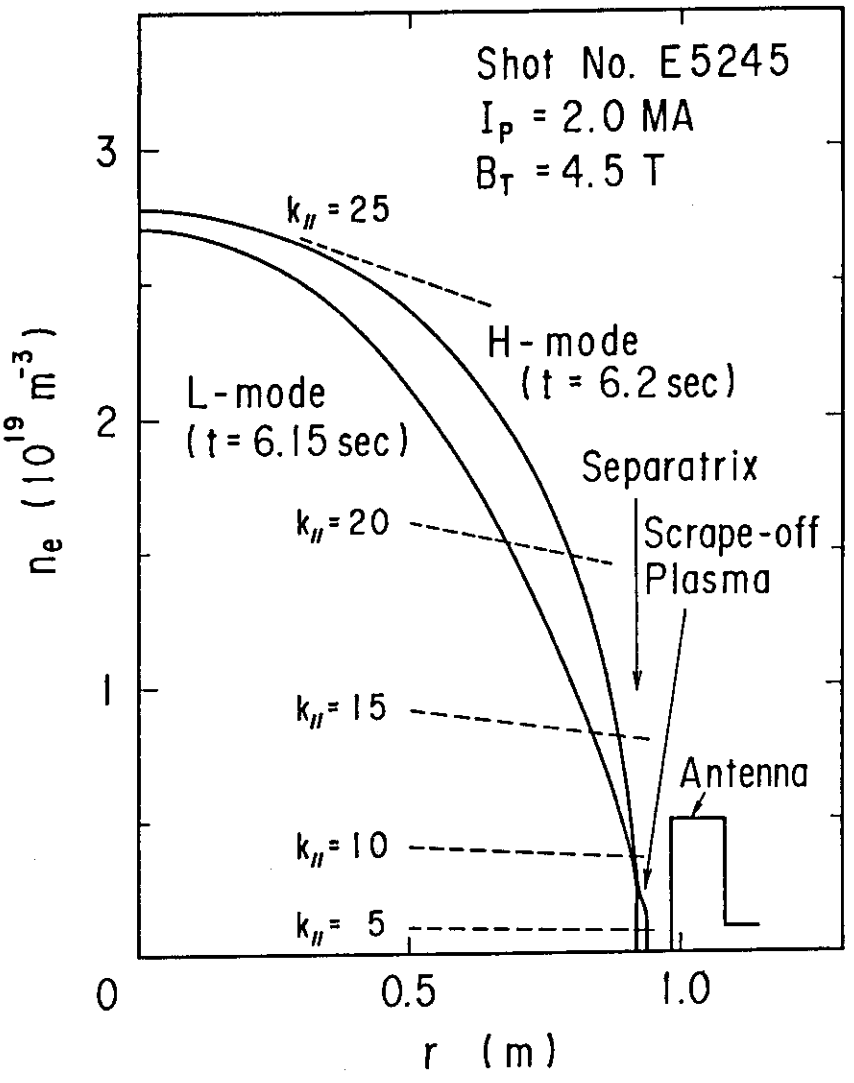

Fig. 16 Electron density profile of L and H modes obtained by functional fitting analysis of the data of three-channel far-infrared laser interferometer. Broken lines indicate fast wave cut-off density for various values of $k_{\parallel}$.